

# A New Anti-Counterfeiting Feature Relying on Invisible Luminescent Full Color Images Printed with Lanthanide-Based Inks

Julien Andres, Roger D. Hersch, Jacques-Edouard Moser, and Anne-Sophie Chauvin\*

Europium and terbium trisdipicolinate complexes are inkjet printed onto paper with commercially available desktop inkjet printers. Together with a commercial blue luminescent ink, the red-emitting luminescent ink containing europium and the green-emitting luminescent ink containing terbium are used to reproduce accurate full color images that are invisible under white light and appear under a 254 nm UV light. Such invisible luminescent images are attractive anti-counterfeiting security features. The luminescent prints have a color range (gamut) nearly as wide as the gamut of a standard sRGB display. The gamut of the luminescent prints is determined by relying on a simple model predicting the relative spectral radiant emittances of any printed luminescent color halftone. The model is also used to establish the correspondence between the surface coverages of the printed luminescent inks and the emitted color of these luminescent halftones. The accuracy of the spectral prediction model is very good and can be rationalized by the absence of quenching when the luminescent lanthanide complexes are printed in superposition with the other luminescent materials.

to authenticate are therefore important for the protection of brands and valuable documents such as bank notes, diplomas and certificates. Luminescent tags or labels are appreciated security elements for protecting authenticatable articles. One way to incorporate luminescent materials as luminescent security elements is to print them with luminescent inks.<sup>[2]</sup> Nowadays, these printed luminescent security elements usually comprise only solid or halftone<sup>[3]</sup> single ink color patterns. Typical examples are bank notes that show luminescent parts under UV light (see Figure S3 in the Supporting Information, SI).

Procedures for producing full color images by printing luminescent inks exist.<sup>[4]</sup> These methods use several luminescent inks with different luminescent colors to form a full color image by luminescence. However, they are either colorimetrically inaccurate or use complex halftoning algorithms.

Many luminescent inks and markers, used for example as security inks, are made of lanthanide compounds.<sup>[5]</sup> The distinctive character of the emission from lanthanide ions, and particularly, their unique spectral fingerprints, enable the use of emissions and colors from lanthanide blends as security labels, markers or tags.<sup>[5d–5f]</sup>

Lanthanide ions are widely recognized for their exceptional luminescence. The forbidden nature of their *ff* transitions and the shielding of the *f* electrons by more extended electronic shells enable achieving narrow spectral lines, which produce pure luminescent colors with long lifetimes.<sup>[6]</sup> Luminescent lanthanide ions are present in phosphors for lighting and display devices. Among the lanthanide series, europium and terbium ions are key elements for producing white light by combining red, green, and blue emissions (additive color synthesis).<sup>[7]</sup> Because of the low probability of their *ff* transitions, the extinction coefficients of the lanthanide ions are very low, about a few  $\text{L mol}^{-1} \text{cm}^{-1}$ . In order to efficiently harvest light and yield an important emission, luminescent lanthanide ions are usually photosensitized by organic chromophores with specific photophysical properties. These chromophores, sometimes called antennae, are embedded in ligands capable of coordinating trivalent lanthanide ions and forming complexes that are kinetically and thermodynamically stable.

Dipicolinic acid (dpa) is a tridentate ligand forming stable tris(dipicolinato) lanthanide complexes under stoichiometric

## 1. Introduction

Counterfeiting is a growing global problem that challenges companies, governments and customers.<sup>[1]</sup> Anti-counterfeiting techniques that make genuine items harder to copy and easier

Dr. J. Andres, Dr. A.-S. Chauvin  
École Polytechnique Fédérale de Lausanne  
Faculté des Sciences de Base  
Institut des Sciences et Ingénierie Chimiques  
BCH 1405, CH-1015, Lausanne, Switzerland  
E-mail: anne-sophie.chauvin@epfl.ch

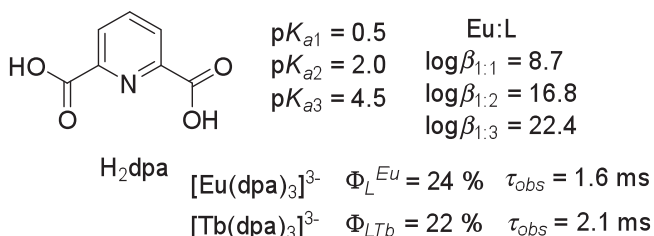
Prof. R. D. Hersch  
École Polytechnique Fédérale de Lausanne  
Faculté Informatique et Communication  
Laboratoire des Systèmes Périphériques  
Station 14, CH-1015, Lausanne, Switzerland

Prof. J.-E. Moser  
École Polytechnique Fédérale de Lausanne  
Faculté des Sciences de Base  
Institut des Sciences et Ingénierie Chimiques  
Groupe de Dynamique Photochimique  
Station 6, CH-1015, Lausanne, Switzerland

This is an open access article under the terms of the Creative Commons Attribution-NonCommercial License, which permits use, distribution and reproduction in any medium, provided the original work is properly cited and is not used for commercial purposes.

DOI: 10.1002/adfm.201400298





**Scheme 1.** Dipicolinic acid: ligand structure,  $\text{pK}_a$  values of the ligand stability constants of its europium and terbium complex with quantum yields and lifetimes in Tris-buffered solution (pH 7.4, 0.1 mM in complex). Values taken from the literature.<sup>[11,12]</sup>

conditions (hereafter trisdipicolinate complexes). The trisdipicolinate lanthanide complexes are water soluble and are stable in water at neutral pH, as shown by the  $\log\beta$  values displayed in **Scheme 1**. They also crystallize at high concentrations and were investigated by X-ray crystallography.<sup>[8]</sup> They display a tricapped trigonal prism structure typical of nine-coordinated ions. The tris structure is retained in aqueous solution at neutral pH, as proved, for example, by the lanthanide induced shifts,<sup>[9]</sup> and by the number of water molecules in the first coordination sphere obtained by measuring the observed lifetime in water and in deuterated water.<sup>[10]</sup> Europium and terbium trisdipicolinate have very attractive photophysical properties with high quantum yields and long lifetimes in the millisecond range (see Scheme 1).

Consequently, they are often used as standards for the determination of quantum yields.<sup>[11]</sup> Lanthanide trisdipicolinate complexes were also the main component of an aqueous inkjet ink composition in a patent application.<sup>[5c]</sup> However, they only absorb below 300 nm. The excitation of the ligand thus requires UV-C, which can be achieved by an uncoated mercury lamp with a UV bandpass filter. There are countless occurrences of dpa lanthanide complexes or complexes with dpa derivatives in the literature. Overviews of the different structures derived from dpa can be found elsewhere.<sup>[7a,13]</sup>

Color reproduction aims at reproducing original images on different media (e.g. prints, photographs, display devices, etc.) with the best possible color fidelity. In the case of prints, color reproduction aims at producing printed images with colors as close as the colors viewed on a display device.<sup>[14]</sup> In order to obtain a visually accurate and faithful reproduction of a color image on prints, a color reproduction workflow is used. This workflow consists of establishing the color domain (gamut) reproducible on the target prints, mapping original colors into printable colors,<sup>[15]</sup> and finding the correspondences between the desired mapped printed colors and the surface coverages of inks.

In this study, we propose to produce luminescent inks based on lanthanide complexes, printing them on paper with a desktop inkjet printer and forming thereby accurately reproduced invisible full color luminescent images. These full color images are visible only under UV light and can be used for anti-counterfeiting purposes. We used lanthanide trisdipicolinate complexes as luminescent dyes in the invisible luminescent inkjet inks and printed them with a commercially available inkjet printer. Since they do not absorb visible light, these inks are invisible. By exciting them with UV light, they become

visible by luminescence. Full color luminescent images under UV light are reproduced by taking advantage of a specially conceived color reproduction workflow. The following luminescent inks are used: a red-emitting luminescent ink composed of europium trisdipicolinate, a green-emitting luminescent ink composed of terbium trisdipicolinate, and a commercially available blue-emitting luminescent ink. This commercial blue luminescent ink was selected because no blue-emitting dipicolinate complex providing a sufficiently high emission intensity was found. This selection of inks also allowed verifying that the luminescent lanthanide inks can be used together with an already existing commercial invisible luminescent ink. The ability of the luminescent lanthanide inks to be superposed with each other is tested first. Then, the three luminescent inks are used to reproduce full color images by luminescence. For that purpose, a model capable of predicting halftone emission spectra as a function of ink surface coverages has been established.

## 2. Results and Discussion

The red-emitting and green-emitting invisible luminescent inks were prepared from europium and terbium trisdipicolinate complexes respectively, as described in the experimental part given in SI. The ink formula prints properly (i.e. the ink is ejected from the printhead and forms visually well printed prints) both with a “bubble-jet” type Canon inkjet printer and with a “micro-piezo” type Epson inkjet printer (see SI for additional information about the printers). Two kinds of paper were used in this study: matte Canson paper and glossy Hahnemühle paper, both without fluorescent optical brightening agents. These papers were chosen for their outstanding quality, uniformity, and printability for inkjet. The procedure is yet also applicable to any non-fluorescent paper that is suitable for inkjet printing.

### 2.1. Effect of the Superposition of the Luminescent Inks

In order to test if the luminescent inks can be superposed with each other without quenching or disruption of the complexes, the inks were printed as solid (fulltone: 100% of surface coverage of the inks) luminescent samples. Time-resolved emission spectra of the lanthanide ions were measured under excitation with a pulsed nanosecond laser at 254 nm.

According to the observed lifetimes fitted from the emission decays, no quenching of the lanthanide ions occurs for the terbium complex, see **Figure 1**. The same behavior was observed with the europium complex. A luminescent ink can therefore be superposed with the other luminescent inks in prints without altering the photophysical properties of the lanthanide trisdipicolinate complexes.

The existing colorimetrically accurate color reproduction workflow developed by Hersch and coworkers was specially adapted to fluorescent inks that may induce quenching effects when the inks are on top of another.<sup>[4a]</sup> Since these luminescent inks are not quenching each other, a simpler procedure was developed.

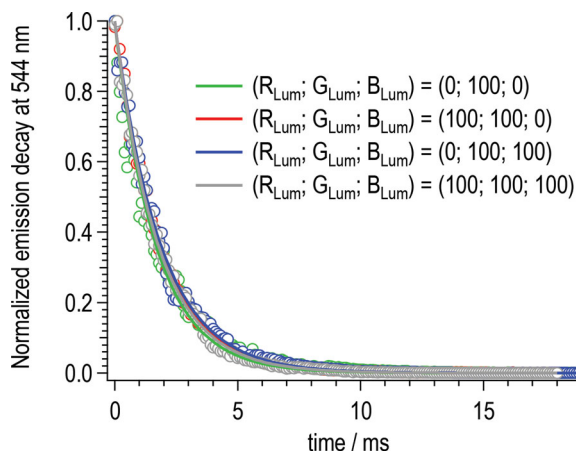


**Figure 1.** Normalized emission decay of the  $^5D_4 \rightarrow ^7F_5$  transition of  $[Tb(dpa)_3]^{3-}$  for the green, yellow, cyan and white luminescent colorants.

## 2.2. Characterization of the Luminescent Halftones and Prediction of Their Emission

In order to confirm that the red-emitting, green-emitting and blue-emitting luminescent inks yield luminescent colors suitable for trichromatic additive color synthesis, we printed them as luminescent halftones and measured their emissions under short wave UV light.

Excited by a 254 nm UV light source, the luminescent halftones were observed under a microscope. Their luminescent halftone structure is shown in **Figure 2**. Firstly, as seen in (B), the solid luminescent samples (surface coverage of 100%) do not entirely cover the surface. There is a regular line-like pattern that can also be observed on magnified solid samples printed with visible inks. This pattern is determined by the arrangement of the print-head nozzles and by other characteristics of the printer and its driver. Secondly, dot gain due to the lateral propagation of light within the substrate and to ink spreading (which is a well-known issue in color reproduction) can be observed in **Figure 2**. Compare the picture (D) of the luminescent color halftone with the ideal shaped luminescent dots shown in picture (E). Dot gain usually increases the effective dot surface coverages. These dot gain phenomena are further illustrated in SI (Figure S4) for the case of luminescent halftones. In order to account for dot gain, ink spreading curves are established which map nominal to effective ink dot surface coverages. This calibration step is performed by relying on a model predicting emission spectra as a function of ink surface coverages. The calibration samples comprise single ink halftones at 25%, 50%, and 75% surface coverages superposed with the bare paper, one ink and two inks.

The model for predicting the emission spectrum of any combination of luminescent ink surface coverages is based on the additive synthesis of emitted colors. As confirmed by **Figure 2**, the superposition of ink halftone dots yields additive colors. For the three luminescent inks, there are eight luminescent colorants that can be generated by superposition: red, green, blue, yellow (red + green), magenta (red + blue), cyan (green + blue), white (red + green + blue), and black (no luminescent ink). The surface coverages of these luminescent colorants define the

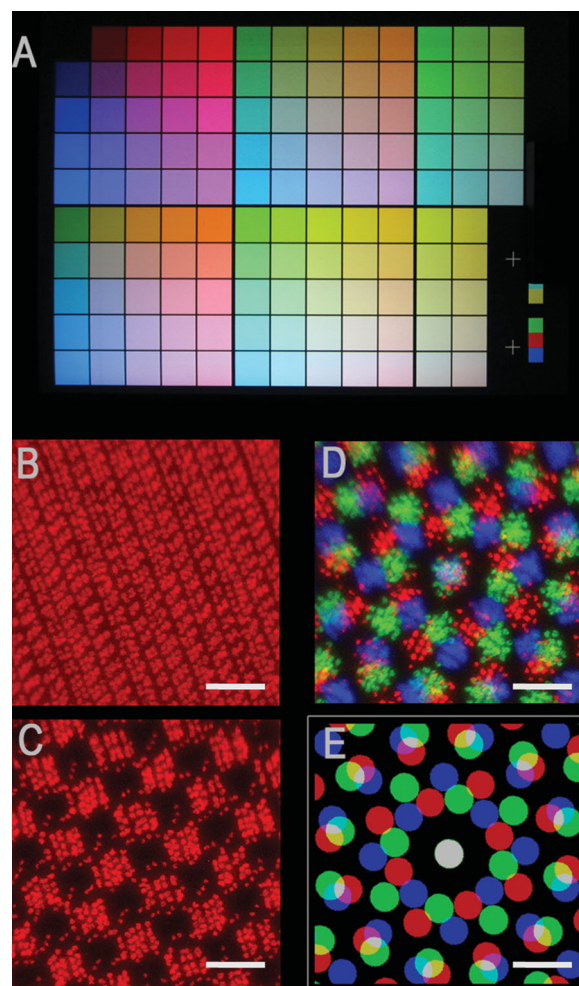


**Figure 2.** (A) Picture under UV light of the 125 luminescent samples printed on the Canson paper and printed by superposing the three luminescent inks at surface coverages from 0 % to 100% by steps of 25%; (B) Picture of the 100 % surface coverage of the red luminescent ink in A seen under a microscope; (C) Picture of the 50% surface coverage of the red luminescent ink in A seen under a microscope; (D) Picture of the luminescent color halftone at surface coverages  $(r, g, b) = (0.25, 0.25, 0.25)$  seen under a microscope; (E) Illustration of the ideally shaped luminescent dots of sample D. The thick white lines correspond to 1/100 of an inch (254  $\mu\text{m}$ ).

intensity of the resulting emittance relative to the emittance of the fulltone luminescent colorant. However, because of an inner filter effect on the luminescent inks (i.e., a decrease of the emission intensity due to the absorption of part of the UV excitation light source by superposed inks), the luminescent colorants produced by superposition of luminescent inks are not exactly the addition of the emission spectra of the superposed luminescent inks. Therefore, the different superpositions of the inks have to be taken into account when summing the emittances. This is done by defining the superpositions of inks as distinct luminescent colorants. **Figure 3** displays the emission spectra of all considered luminescent colorants, as well as the excitation spectra of the red, green and blue luminescent colorants. At the top of **Figure 3**, the base colorants are formed by the single luminescent inks printed as solid samples. In the



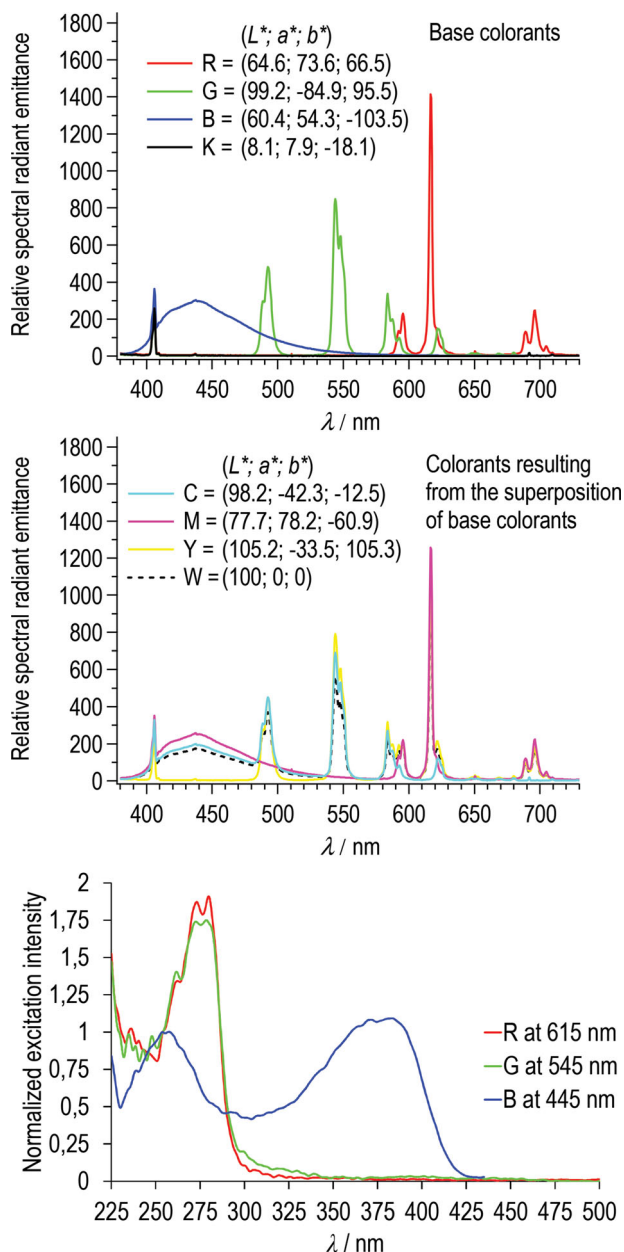


**Figure 3.** Top: Relative spectral radiant emittances,  $E_f(\lambda)$  used in Equation (1) under excitation at  $\lambda_{\text{ex}} = 254$  nm, for the Canson Rag Photographique paper. The top graph shows the luminescent base colorants formed by the red emitting  $\text{Na}_3[\text{Eu}(\text{dpa})_3]$  4.5%w ink solution, the green emitting  $\text{Na}_3[\text{Tb}(\text{dpa})_3]$  5%w ink solution, the blue emitting commercial cyan Firefly ink and the unprinted paper black colorant. The graph in the middle shows the luminescent colorants obtained by superposing the R, G and B colorants. Bottom: Excitation spectra of the red, green and blue luminescent colorants (R, G, B) for their maximum emission at 615 nm, 545 nm and 445 nm respectively, normalized at 254 nm.

middle of Figure 3, the solid colorants resulting from the superposition of luminescent inks are shown. The bottom of Figure 3 shows the excitation spectra of the luminescent inks printed on Canson paper. These excitation spectra indicate that a UV light source at 254 nm (UV bandpass filtered uncoated mercury light) is suited for exciting all three luminescent inks, whereas

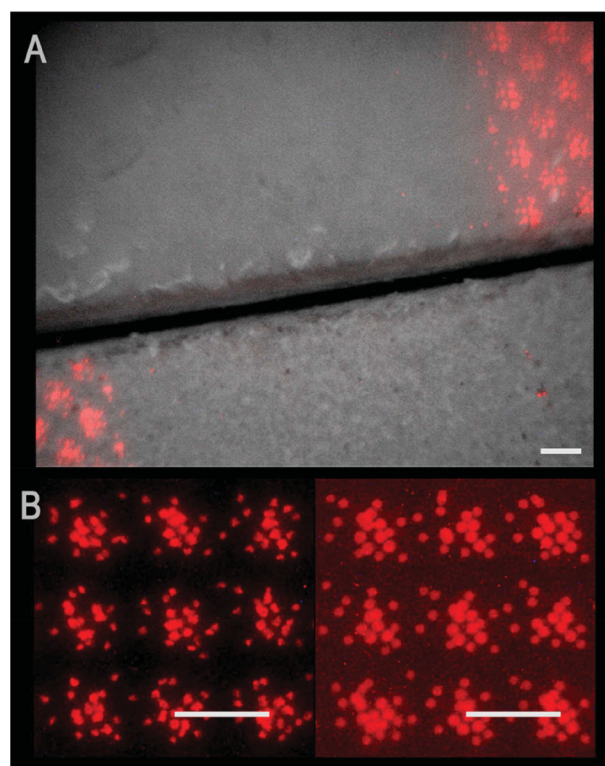


**Figure 4.** (A) Superposed picture of cut samples of the 25% surface coverage red luminescent halftone printed on the Canson paper (bottom, rough paper surface) and on the Hahnemühle paper (top, smooth paper surface) with the desaturated picture of the same sample observed under white light. (B) 3×3 cluster of screen elements showing different dot gains for the 25% surface coverage red luminescent halftone printed on the Canson paper (left) and on the Hahnemühle paper (right). The thick white lines correspond to 1/100 of an inch (254  $\mu\text{m}$ ).

a UV light source at 366 nm is only capable of exciting the blue luminescent ink.

Equation (1) predicts the emission spectrum (total relative spectral radiant emittance) of a luminescent halftone  $E(\lambda)$ , as the sum of the respective relative spectral radiant emittances  $E_f(\lambda)$  of the eight luminescent solid colorants  $f$ , weighted by their surface coverages  $a_f$ . This spectral prediction model is similar to the spectral Neugebauer model used for predicting the reflectance spectra of color halftones.<sup>[16]</sup>

$$E(\lambda) = \sum_{f=1}^8 a_f \cdot E_f(\lambda) \quad (1)$$

Figure 4 shows the two studied papers viewed under a microscope and the impact the paper has on the luminescent halftones. On the matte rough surface of the Canson paper, the red luminescent halftone dots look more irregular than on the glossy smooth surface of the Hahnemühle paper. In addition, the glossy Hahnemühle paper seems to have more optical dot gain as seen by the red background compared to the much blacker one on the Canson paper. This observation is important since it indicates that luminescent halftones could be an efficient tool to investigate and characterize paper properties that are impossible to measure with normal color inks.

Besides the paper properties, dot gain also depends on the superposition of the inks. Therefore, a dot gain calibration needs to be established for each superposition condition. For three inks, the following cases are considered: each ink halftone alone, each ink halftone superposed with a second ink, and each ink halftone superposed with the two other inks. There are therefore twelve superposition conditions, which yield twelve dot gain curves.<sup>[17]</sup> Dot gain curves are obtained by subtracting the nominal surface coverages from the effective surface coverages. The effective surface coverages used to determine the dot gain curves are obtained by calibration, as reported in the experimental part (see SI). The resulting dot gain curves for each luminescent ink halftone superposed with paper, with one fulltone luminescent ink and with two fulltone luminescent inks are shown in SI (Figure S5). These dot gain curves depend on the paper and on the ink on which the halftone dot is superposed.

Once calibrated, the model was tested by comparing the predicted colors with the measured color on a set of samples representing the 125 combinations of 0%, 25%, 50%, 75% and 100% nominal surface coverages of the three inks (Figure 2A). This was done by measuring the relative spectral radiant emittances of the 125 luminescent samples, predicting the corresponding spectral radiant emittances according to Equation (1), converting the predicted and measured spectral radiant emittances to the CIE-XYZ color space and then to the CIELAB color space, and calculating the CIELAB  $\Delta E_{94}$  color differences between the predicted and measured CIELAB colors. The reference white chosen for converting the CIE-XYZ tristimulus values to CIELAB colors was the luminescent white colorant formed by the superposition of the three inks. The CIELAB  $\Delta E_{94}$  color differences between the measurements and the predictions give the accuracy of the prediction. The lower the  $\Delta E_{94}$  color difference, the better the accuracy. Additional information about CIE-XYZ, CIELAB and the  $\Delta E_{94}$  color difference can be found in the literature.<sup>[14]</sup> The equations used to calculate the colorimetric values are presented in SI.

The detailed procedure for predicting emission spectra from nominal surface coverages of the luminescent inks is described in the experimental part (see SI). This procedure was applied to both papers. The  $\Delta E_{94}$  color differences between the predicted and the measured colors were then calculated. For both papers, the distribution of the  $\Delta E_{94}$  color differences between the emission predictions and the measurements for the 125 tested luminescent samples (see Figure 5) has an average  $\Delta E_{94}$  value of 0.9 and a 95% quantile around 2.0. The maximal  $\Delta E_{94}$  value is 3.1 on the Canson paper and 2.5 on the Hahnemühle paper. Since the average color difference between predicted and measured color samples is below 1.0 (visibility limit of the human visual system), the prediction accuracy of our model is excellent on both papers.

Such a good accuracy can be rationalized by the inertness of the lanthanide trispicolate complexes when printed on top

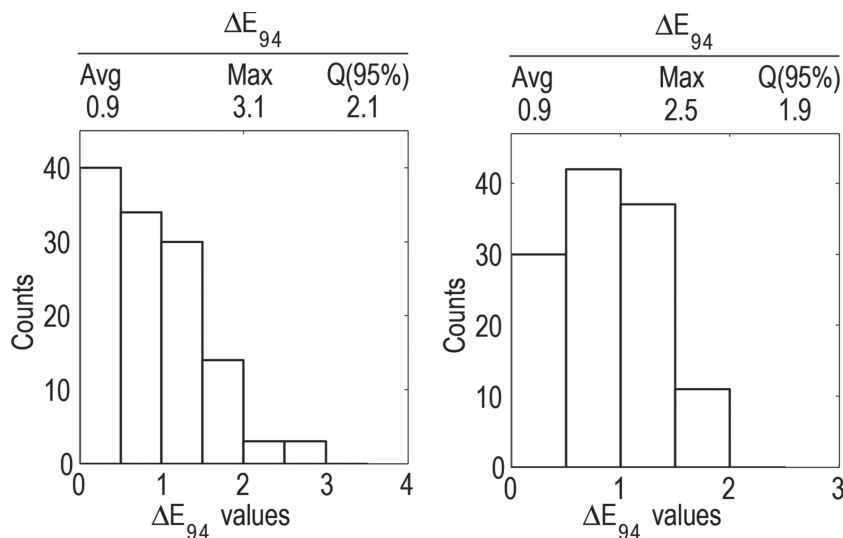


**Figure 5.** Distribution of the color differences between the measured and the corresponding predicted CIELAB colors on the Canson Rag Photographique paper (left) and on the Hahnemühle Photo Rag Baryta paper (right) with average (avg) maximum (max) and 95%-quantile values.

of each other or on the blue luminescent ink. The inner filter effect, which results in a lower emission intensity when superposing the inks, is not problematic since it is taken into account by measuring the emittances of the luminescent colorants (see Figure 3).

The prediction accuracy demonstrates that our ink formula yields halftones that are suitable for color reproduction. In addition, the good behavior of our custom inks proves that they are compatible with existing commercial inks and printers.

Since the model is accurate, the emission spectrum and hence the luminescent color of any luminescent halftone can be predicted precisely. The gamut of the colors spanned by the luminescent ink halftones can thus be determined from predicted luminescent colors. The spectral prediction model can also be used to find the surface coverages of the three luminescent inks that create a desired luminescent color under the UV bandpass filtered uncoated mercury light.

### 2.3. Visualization of the Color Range Offered by the Luminescent Inks

In order to determine the gamut (reproducible color range) of the luminescent ink halftones, the emittance of each combination of the surface coverages of the inks by steps of 2.5% of nominal surface coverage was first predicted, converted to CIE-XYZ tristimulus values, and then to CIELAB colors. The reference white is given by the emittance of the white luminescent colorant formed by the solid superposition (100 % surface coverages) of the three inks. From the resulting 68 921 CIELAB colors, the gamut boundary was computed by applying a Delaunay triangulation and then the ball-pivoting algorithm developed by Bernardini et al.<sup>[18]</sup> The spectral prediction model enabled us to calculate the 68 921 spectra instead of measuring them.

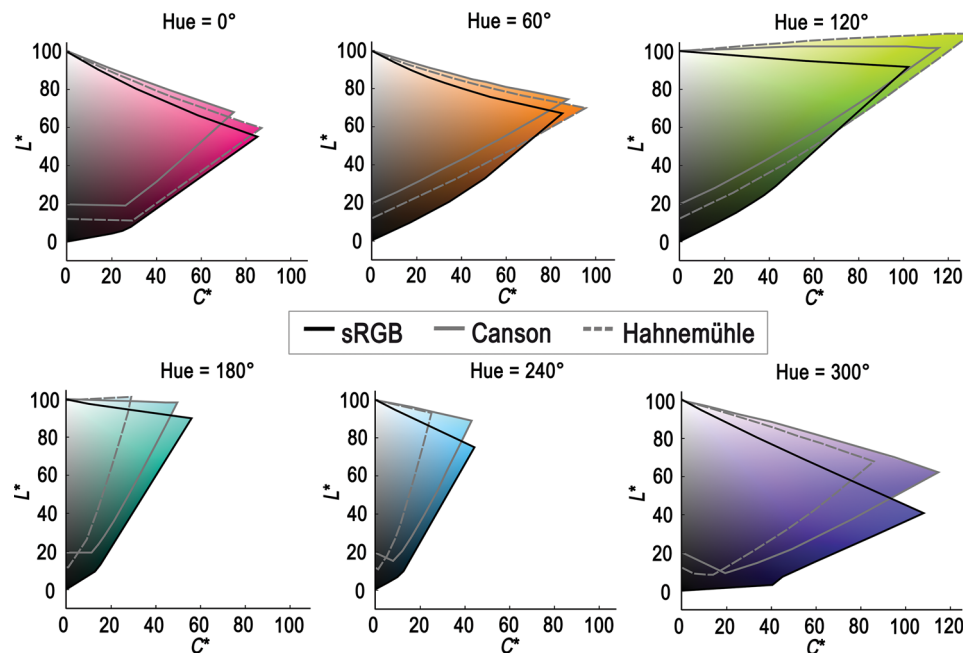


**Figure 6.** Gamut of the sRGB display colors and of the luminescent ink colors composed of  $\text{Na}_3[\text{Eu}(\text{dpa})_3]$ ,  $\text{Na}_3[\text{Tb}(\text{dpa})_3]$  and an unknown blue emitting compound printed on the Canson and on the Hahnemühle papers, displayed in the CIELAB color space.

As shown in **Figure 6**, the gamut of the luminescent ink halftones depends on the substrate on which they are printed. Furthermore, the white luminescent colorant used as the reference white color is different on the two papers. On the Canson paper, the white luminescent color looks more reddish than on the Hahnemühle paper. The white chromaticity is  $(x, y) = (0.31, 0.29)$  on Canson paper and  $(x, y) = (0.27, 0.28)$  on Hahnemühle paper. This may be explained by the following phenomena: the printed ink dots may penetrate and diffuse more or less in the paper, and the exciting UV light scattered by the paper may be subject to different inner filter effects depending on the ink superposition condition. Paper properties such as the coating, the glossiness, the scattering of the excitation UV light inside the paper, etc. may thus have an impact on the absorption of UV light by the individual inks and therefore induce different emissions of the ink dots forming the color halftones.

The colors of digital color images are generally defined in the sRGB color space that encloses the colors reproducible by standard sRGB display devices. **Figure 6** shows both the gamut of a standard sRGB display and the gamut of the luminescent inks in the CIELAB color space. The gamut of the luminescent inks is close to the sRGB gamut in most hues, except in the blue colors where it is significantly smaller. Because of the inner filter effect that decreases the emission intensity of the colorants formed by superposed inks, the emission intensity of the white (superposition of the three inks) is lower than the emission intensity of the other colorants (**Figure 3**, right part). As a result, some colors with a green component have luminances higher than  $Y = 100$ , and hence, a lightness higher than  $L^* = 100$ . For the Canson paper, the yellow colorant has a lightness  $L^* = 105.2$ . For the Hahnemühle paper, the green ( $L^* = 109.7$ ), yellow ( $L^* = 108.9$ ) and cyan ( $L^* = 101.3$ ) colorants have lightnesses higher than the lightness of the white. Therefore,

at high lightnesses, the gamut in the green hues (with hue angles around  $h_{ab} = 135^\circ$ ) is larger than the corresponding sRGB gamut. This is also true, yet to a smaller extent, for the other hues.

Finally, the gamut of the luminescent inks does not include as many dark colors as the sRGB gamut. The lowest lightness on the greyscale axis achievable with the luminescent ink halftones is between 10 and 20. However, such dark colors are darker than the ones obtained in subtractive color synthesis by classical cyan, magenta and yellow inkjet inks. Let us also note that the unprinted paper does not look black, but bluish due to the reflection of a strong peak from the mercury lamp at 406 nm, despite the presence of a UV bandpass filter. This is confirmed by the fact that the lowest  $L^*$  values are in the blue-violet hues.

#### 2.4. Printing Invisible Pictures with the Luminescent Inks

Due to the large gamut of the luminescent inks, nice vivid images are expected with only little color differences between the input images viewed on an sRGB display and those observed under UV excitation. In order to print with the luminescent inks a faithful reproduction of a color image, the surface coverages of the luminescent inks enabling printing a given color are obtained by accessing a 3D lookup table that was constructed with the help of the spectral prediction model (detailed procedure in the experimental part). These surface coverages enable creating the red, green and blue luminescent ink separation layers. These separation layers are then halftoned according to the same method than the one used in the calibration of the spectral prediction model, i.e. with a classical rotated screen, having a round shape, at a screen frequency of





**Figure 7.** Photographs of a set of standard images reproduced with the luminescent inks on the Canson paper. On the left, a printed paper sheet under an A illuminant: the luminescent image is invisible. On the center, the same printed paper sheet under UV excitation at 254 nm: the luminescent images produced by the emission of the lanthanide complexes and of the blue emitting compound are visible and accurately reproduced. On the right, enlargements of the ski picture shown in the photograph on the center (i.e. viewed under UV light).

100 lpi, at orientations of 75° for the blue luminescent ink, 45° for the red luminescent ink and 15° for the green luminescent ink for the target printer resolution of 720 dpi. The halftoned luminescent ink layers are then printed on the corresponding paper with the Epson Stylus Photo P50 inkjet printer.

**Figure 7** displays a picture taken by a Canon PowerShot S95 digital camera of three standard images printed with the luminescent inks on the Canson paper. These three images represent a wide range of natural colors in the fruits, of saturated colors in the ski picture, and of people with skin tones in the orchestra image. They provide a good indication of the quality of the color reproduction. Additional photographs of the resulting luminescent images are presented as SI (Figures S6–S8).

### 3. Conclusions

For the first time, invisible full color luminescent images have been reproduced faithfully by printing luminescent inks containing lanthanide ions. The superposition of the europium and terbium trisdipicolinate inks enables reproducing colors from red to orange, yellow and green. The red emitting and green emitting luminescent inks were synthesized by diluting europium and terbium trisdipicolinate in a simple aqueous formula suitable for inkjet printing. In order to enable trichromatic additive color synthesis, the present lanthanide based red and green emitting inks are complemented by a commercial blue emitting luminescent ink.

The color reproduction workflow has been adapted to luminescent prints. The proposed simple spectral radiant emittance model predicting the emission of the printed luminescent halftones is accurate. This may be due i) to the stability and

photophysical properties of the lanthanide complexes, and ii) to the fact that the color reproduction workflow comprises the measured emission spectra of the new colorants formed by the superpositions of the solid luminescent inks. The shadowing of the excitation light induced by the superpositions of the inks is thus taken into account.

The color gamut of the luminescent inks is wide and includes high chroma colors. At high lightnesses, it is larger than the sRGB gamut of a standard display device. The dark tones are not as dark as the ones of sRGB displays. However, they have a darkness similar to the one offered by classical inkjet printers. The images printed with the luminescent inks are pleasant and have a similar look as the images viewed on an sRGB display.

The potential of this application as anti-counterfeiting feature is attractive. Tagged documents can be easily authenticated by visualization under UV light. This document security feature cannot be counterfeited without the appropriate luminescent inks, and without the color reproduction software.

The color reproduction workflow and characterization procedure established in this work can be applied to other luminescent inks. Therefore, it provides a unique tool for the development of security features relying on luminescent prints.

In the future, we may consider the synthesis of a blue luminescent ink instead of the utilization of a commercial product. Complexes capable of sensitizing thulium and complexes with non-luminescent lanthanide ions have shown potential blue components in white light generation.<sup>[19]</sup> The sensitization of thulium has yet serious limitations.<sup>[20]</sup> We may thus turn towards blue ligand-centered emissions. Furthermore, the synthesis of new ligands capable of being excited at higher wavelengths may improve future luminescent dyes.

Regarding the cost of the luminescent inks, dipicolinic acid is commercially available and cheap (no need for a

time-consuming and expensive synthesis). It is therefore an excellent ligand because of its properties and availability. Lower purity lanthanide salts could also be used as long as no luminescent impurities change the emitted colors.

## Supporting Information

Supporting Information is available from the Wiley Online Library or from the author.

## Acknowledgements

The authors would like to thank Romain Rossier for his help and advice on colorimetry and for providing some of the matlab software modules further developed and used in this study. This study has been partly financed by the Swiss National Science Foundation, grants 200020\_126757 and 200021\_143501.

Received: January 27, 2014

Revised: March 12, 2014

Published online: May 22, 2014

- [1] OECD, *The Economic Impact of Counterfeiting and Piracy*, OECD Publishing, Paris, Paris, **2008**.
- [2] R. L. Van Renesse, *Optical Document Security*, Artech House, Boston **2004**.
- [3] Halftoning converts continuous tone levels to ink dot surface coverages. When the size of the halftone dots is small, the halftone is perceived by a human viewer as a continuous tone. For more information, see C. Hains, S.-G. Wang, K. Knox, in *Digital Color Imaging Handbook* (Ed: G. Sharma), CRC Press, Boca Raton **2003**, pp. 385–490.
- [4] a) R. D. Hersch, P. Donze, S. Chosson, *Acm. T. Graphic*, **2007**, article 75; b) W. J. Coyle, J. C. Smith, Angstrom Technologies, Inc., US Patent 7821675, 2010.
- [5] a) J. D. Auslander, W. Berson, Pitney Bowes, US Patent 5542971, **1996**; b) B. A. Lent, G. G. Deng, J. F. Ezpeleta, The General Electric Company, Plc, WO 97/10307, **1997**; c) V. Aboutanos, T. Tiller, C. Reinhard, S. Rascagnères, SICPA Holding SA, US Patent 8,685,276, **2010**; d) G. A. Ross, P. Pollard, C. Hunter, S. Officer, G. R. Prabhu, NRC Corporation, US Patent, 7,129,506, **2004**; e) S. Officer, G. R. Prabhu, P. Pollard, C. Hunter, G. Ross, *Proc. SPIE-IS&T Electronic Imaging* **2004**, 5310, 387–395; f) G. Kaur, Y. Dwivedi, A. Rai, S. B. Rai, *Spectrochim. Acta A: Mol. Biomol. Spectr.* **2012**, 95, 511–516; g) Y. Liu, K. Ai, L. Lu, *Nanosci.* **2011**, 3, 4804–4810; h) J. M. Meruga, W. M. Cross, P. S. May, Q. Luu, G. A. Crawford, J. J. Kellar, *Nanotech.* **2012**, 23, 395201.
- [6] J. Andres, A. S. Chauvin, in *The Rare Earth Elements: Fundamentals and Applications* (Ed: D. A. Atwood), John Wiley & Sons Ltd, Chichester, UK **2012**, pp.111–133.
- [7] a) S. V. Eliseeva, J. C. G. Bunzli, *Chem. Soc. Rev.* **2010**, 39, 189–227; b) S. V. Eliseeva, J. C. G. Bunzli, *New J. Chem.* **2011**, 35, 1165–1176; c) L. D. Carlos, R. A. S. Ferreira, V. de Zea Bermudez, B. Julián-López, P. Escrivano, *Chem. Soc. Rev.* **2011**, 40, 536–549.
- [8] a) L. VanMeervelt, K. Binnemans, K. VanHerck, C. GorllerWalrand, *B. Soc. Chim. Belg.* **1997**, 106, 25–27; b) P. A. Brayshaw, J. M. Harrowfield, A. N. Sobolev, *Acta Crystallogr. C* **1995**, 51, 1799–1802.
- [9] a) C. N. Reilly, B. W. Good, *Anal. Chem.* **1975**, 47, 2110–2116; b) H. Donato, R. B. Martin, *J. Am. Chem. Soc.* **1972**, 94, 4129–4131.
- [10] a) W. D. Horrocks, Jr., D. R. Sudnick, *Acc. Chem. Res.* **1981**, 14, 384–392; b) A. Beeby, I. M. Clarkson, R. S. Dickins, S. Faulkner, D. Parker, L. Royle, A. S. de Sousa, J. A. G. Williams, M. Woods, *J. Chem. Soc., Perkin Trans.* **1999**, 493–503; c) M. Supkowski, W. D. Horrocks, *Inorg. Chim. Acta* **2002**, 340, 44–48.
- [11] A. S. Chauvin, F. Gumy, D. Imbert, J. C. G. Bunzli, *Spectrosc. Lett.* **2004**, 37, 517–532.
- [12] A. L. Gassner, C. Duhot, J. C. G. Bunzli, A. S. Chauvin, *Inorg. Chem.* **2008**, 47, 7802–7812.
- [13] a) K. Binnemans, *Chem. Rev.* **2009**, 109, 4283–4374; b) J. Andres, A. S. Chauvin, in *The Rare Earth Elements: Fundamentals and Applications* (Ed: D. A. Atwood), John Wiley & Sons Ltd, Chichester, UK **2012**, pp.135–152.
- [14] a) G. Sharma, in *Digital Color Imaging Handbook* (Ed: G. Sharma), CRC Press, Boca Raton **2003**, pp.1–114; b) H. G. Völz, in *Industrial Color Testing*, 2nd Ed., Wiley-VCH Verlag GmbH & Co. KGaA, Weinheim **2002**, pp.15–39.
- [15] J. Morovic, in *Digital Color Imaging Handbook* (Ed: G. Sharma), CRC Press, Boca Raton **2003**, pp.639–685.
- [16] J. A. S. Viggiano, *TAGA/ISCC Proc.* **1990**, 44–62.
- [17] R. D. Hersch, F. Crete, *IS&T/SPIE Electronic Imaging Symposium, Color Imaging X* **2005**, 5667, 434–447.
- [18] F. Bernardini, J. Mittleman, H. Rushmeier, C. Silva, G. Taubin, *IEEE Trans. on Vis. and Comp. Graph.* **1999**, 5, 349–359.
- [19] B. W. Ennis, S. Muzzioli, B. L. Reid, D. M. D'Alessio, S. Stagni, D. H. Brown, M. I. Ogden, M. Massi, *Dalton Trans.* **2013**, 42, 6894–6901.
- [20] O. A. Blackburn, M. Tropiano, T. J. Sørensen, J. Thom, A. Beeby, L. M. Bushby, D. Parker, L. S. Natrajan, S. Faulkner, *Phys. Chem. Chem. Phys.* **2012**, 14, 13378–13384.